Chemistry Africa (2026) 9:114
https://doi.org/10.1007/s42250-026-01595-y

ORIGINAL ARTICLE

# Revitalizing Battery Waste: Unveiling Ni/PPy/TiO2-Nanocomposites for Dye Degradation

**Chitranjan Bharti[1] · Anjul Singh[1] · Vidivay[1] · Shruti Baghel[1,2] · Keshari Nandan[1,3]**

Received: 18 July 2025 / Accepted: 5 January 2026
© The Tunisian Chemical Society and Springer Nature Switzerland AG 2026

## Abstract

The rapid growth in electronic waste (e-waste) and the escalating pollution of wastewater are pressing global concerns necessitating sustainable solutions. This study focuses on the synthesis and characterization of Ni doped PPy/TiO2 Nanocomposites (NCs) emphasizing their potential for both photodegradation and electrolytic degradation applications within the context of managing e-waste. Ni nanoparticles (NPs) were extracted from discarded batteries, while TiO2-NPs were green-synthesized from sugarcane husk, aligning with sustainable practices. Polypyrrole (PPy) served as a conductive matrix for these NCs. Comprehensive characterization of Ni/PPy/TiO2-NCs and PPy/TiO2-NCs via UV-Vis spectroscopy, XRD, FT-IR, TGA, EDX, TEM and electrical conductivity measurements confirmed the formation and properties of both NCs. Notably, the Ni/PPy/TiO2-NCs displayed a diminished optical band gap (Eg) of 2.12 eV and a crystallite size of 22.69 nm indicative of their robust thermal stability with 25.1% char residue at 1000 °C. Additionally, they exhibited ohmic behaviour and augmented DC conductivity (3.25 at 100 V) compared to their constituent elements, hinting at their promising electronic applications. The nanocomposites demonstrated superior photocatalytic activity under sunlight, degrading 99.5% of Rose Bengal dye within 4 min compared to 79.57% achieved by TiO2 alone. Additionally, Ni/PPy/TiO2-NCs exhibited excellent electrochemical degradation efficiency, completely eliminating the RB redox peak within 30 min. These results underscore the dual-mode degradation capability of Ni/PPy/TiO2-NCs, positioning them as promising candidates for sustainable environmental remediation strategies. This study highlights the potential of these nanocomposites to address both e-waste management and wastewater treatment challenges effectively.

✉ Chitranjan Bharti
chitranjaniitr@gmail.com

Anjul Singh
Anjulsingh1212@gmail.com

Vidivay
Vidivaysingh@gmail.com

Shruti Baghel
shrutibaghelksj@gmail.com

Keshari Nandan
keshari.gkv@gmail.com

[1] Department of Chemistry, Dharma Samaj College, UP-202001 Aligarh, India

[2] Department of Chemistry, Ganjdundwar College, Ganjdunwara, UP 207242, Kasganj, India

[3] Department of Chemistry, Gurukul Kangri Vishwavidyalaya, Haridwar , India

Published online: 06 March 2026

**Graphical Abstract**

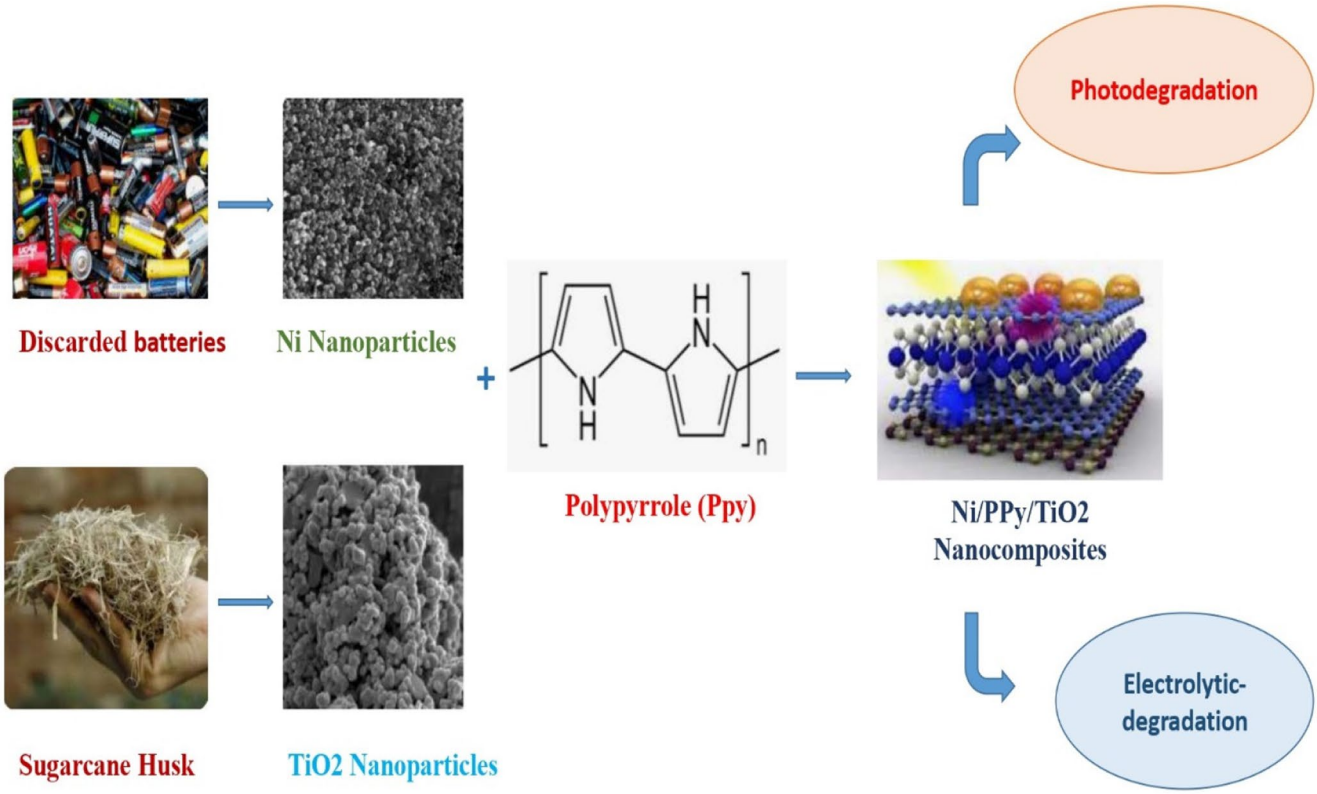


**Keywords** Ni/PPy/TiO2-NCs · RB dye · Photodegradation · Electrochemical degradation

## 1 Introduction

The management and recycling of electronic waste (e-waste) pose significant environmental and health challenges globally [1]. The rapid advancement of technology leads to the frequent disposal of electronic devices, contributing to the growing e-waste problem. E-waste contains hazardous substances such as heavy metals, flame retardants, and other toxic chemicals that can leach into the environment, contaminating soil and water sources [1–3]. Additionally, improper disposal and incineration of e-waste can release harmful substances into the atmosphere, posing serious health risks to humans and wildlife [4]. Moreover, e-waste often contains valuable metals and materials that can be repurposed for various applications, highlighting the importance of efficient recycling and upcycling methods to mitigate these negative impacts [5]. In tandem with e-waste management, addressing the issues of wastewater contamination is critical global priorities [6]. Industrial activities, agricultural practices, and urbanization contribute to the release of harmful dyes, chemicals, and pollutants into water bodies, necessitating effective solutions for wastewater treatment [7]. These pollutants, if not adequately treated, can lead to severe ecological and human health consequences, including the disruption of aquatic ecosystems, bioaccumulation of toxins in the food chain, and the proliferation of waterborne diseases. Nanotechnology emerges as a promising solution to these multifaceted challenges, offering unique properties and functionalities at the nanoscale that can be leveraged for environmental and biomedical applications [8, 9]. Nanomaterials exhibit distinct physical, chemical, and biological properties that differ significantly from their bulk counterparts, enabling them to interact with biological systems and environmental pollutants in novel ways. Specifically, nickel (Ni) and polymers such as polypyrrole (PPy) play pivotal roles in enhancing the performance of nanocomposites [10]. Nickel nanoparticles exhibit excellent electrical conductivity, magnetic properties, and catalytic activity, making them suitable for a wide range of applications, including catalysis, energy storage, and environmental remediation [11, 12]. Polypyrrole (PPy), a conducting polymer, provides a flexible and conductive matrix that can encapsulate other nanoparticles, improving their stability, dispersion, and overall functionality. PPy is known

for its high electrical conductivity, environmental stability, and ease of synthesis, making it an attractive material for various applications, including sensors, actuators, and energy devices [13]. The incorporation of PPy into nanocomposites can enhance their mechanical properties, thermal stability, and electrical performance, thereby broadening their potential applications [14]. Additionally, Titanium dioxide (TiO2) is widely recognized for its photocatalytic properties, making it a valuable component in environmental remediation and biomedical applications [15]. TiO2 can efficiently absorb ultraviolet (UV) light and generate reactive oxygen species (ROS) such as hydroxyl radicals and superoxide anions, which can degrade organic pollutants and dyes in wastewater through photocatalytic oxidation [16]. The incorporation of TiO2into nanocomposites can significantly enhance their photocatalytic efficiency [17, 18]. Moreover, when derived from sustainable sources such as sugarcane, TiO2 contributes to green and waste management practices, aligning with the principles of sustainable development and circular economy. This study delves into the synthesis and characterization of Ni/PPy/TiO2-NCs, emphasizing their potential for photodegradation applications within the context of managing electronic waste. The multifunctional potential of nanotechnology in addressing global environmental and health challenges highlights its role in advancing sustainable and green nanotechnological solutions for healthcare and environmental applications.

## 2 Materials

### 2.1 Chemicals Required

Dimethyl sulfoxide (DMSO) obtained from Sigma Aldrich (Catalog Number: D2650) was used as a solvent for dissolving compounds during experiments and stored at room temperature (20 to 25 °C. Hydrochloric acid (HCl) from Merck (Catalog Number: 100317) and sodium hydroxide (NaOH) from Sigma Aldrich (Catalog Number: S5881), polypyrrole and Titanium tetraisopropoxide Ti[OCH(CH3)2]4) was obtained from Aldrich, A.C.S. Reagent, Old batteries were utilized for nickel extraction.

### 2.2 Plant Material

Sugarcane husk was collected from local fields in Uttar Pradesh, India. The plant material was processed to isolate specific components relevant to the experimental procedures. This involved cleaning, drying, and grinding the sugarcane husk into a fine powder.

### 2.3 Methodology

The synthesis of Ni/PPy/TiO2-NCs begins with the extraction of nickel from discarded batteries. Disassembled battery components are immersed in conc. hydrochloric acid (HCl) solution (37%) and heated at 80 °C for 2 h to dissolve the nickel content [19, 20]. The solution is then filtered to remove undissolved impurities. Sodium hydroxide (NaOH) solution (1 M) is added dropwise to the filtrate until the pH reaches 10, causing nickel hydroxide (Ni(OH)2) to precipitate. The Ni(OH)2 precipitate is filtered, washed with distilled water, and calcined at 100 °C for 6 h in oven to obtain nickel oxide (NiO). Finally, NiO is reduced to nickel nanoparticles by heating in a hydrogen atmosphere at 450 °C for 3 h. From 10 g of spent battery material, 1.26 g of metallic Ni was recovered, corresponding to a recovery efficiency of 12.6% [21]. Simultaneously, The green synthesis of TiO2 nanoparticles using sugarcane husk involves collecting, washing, and drying the husk at 60–70 °C, followed by acid treatment (1:10 HCl) and overnight stirring [22]. The mixture is filtered, and the liquid extract is evaporated to a thick syrup with a pH of 6.7–6.9. Titanium tetraisopropoxide (TTIP) is mixed with ethanol (1:4 ratio) and hydrolysed with HCl while stirring for 1 h. The TTIP solution is combined with the sugarcane husk extract and stirred for several hours. The reaction mixture is incubated at 70 °C with constant stirring, changing from pale yellow to an intense yellow, indicating TiO2 nanoparticle formation. The mixture is then evaporated at 110 °C to yield a thick yellow residue, which is washed with DDW centrifuged twice at 16,000 rpm for 20 min, and dried in an oven to obtain powdered TiO2 nanoparticles. This eco-friendly method leverages agricultural waste, minimizing harmful chemical use. For the synthesis of the Ni/PPy/TiO2-NCs, polypyrrole (PPy) is used directly as a conducting matrix. The TiO2- nanoparticles are dispersed in distilled water using an ultrasonic homogenizer at 20 kHz for 30 min. This dispersed TiO2 solution is then added to the PPy matrix in a weight ratio of 1:2 (TiO2:PPy). Ni-NPs are subsequently introduced to the mixture, and ultrasonic dispersion is continued for an additional 30 min. The resulting mixture is stirred at room temperature for 24 h to ensure thorough mixing and interaction between the components [23, 24].

## 3 Instrumentation and Characterization

The XRD patterns of Crystallographic phase of NCs was recorded over Philips 1700 X-ray diffractometer operating at 40 kV and 30 mA with Cu-Kα radiation at 2θ range of 0° to 90°. Fourier transform infrared spectroscopy (FT-IR) is determined over Perkin Elmer spectrophotometer

through KBr, at wavenumber ($cm^{-1}$) ranging 4000 to 400 under transmission mode. Thermogravimetric analysis was recorded over simultaneous TG-DTG over the EXSTAR TG/DTA 3600 instrument at temperature ranging of 35–1000 °C at heating.

rate of 5 °C/min. DC conductivity was recorded over Keithley's four-probe conductivity meter instrument at room temperature. Microstructural study of the prepared PCPs was investigated using transmission electron microscopy (TEM) on a JEOL JEM-2100 F instrument, with an electron beam accelerated to 200 kV. Electrochemical study was recorded over Potentiostat Galvanostat in a 0.1 M KOH solution over glassy carbon electrode (GCE) as working electrode, Ag/AgCl as reference and a platinum foil as auxiliary electrode.

## 4 Results

### 4.1 UV Spectra and XRD Analysis

UV–vis absorbance spectra and band gap adsorption edges of PPy/TiO2 and Ni/PPy/TiO2- NCs are presented in Fig. 1a. Absorbance spectra reveals about the red shift in wavelength maxima (nm) of PPy/TiO2 from 325 to 376 nm on addition of 5wt% Ni. The absorptions of PPy/TiO2 samples extended to the visible region on increasing the concentration of Ni and maximum absorption 376 nm which is similar to earlier report [25]. The band gap energies of all samples were calculated from Tauc plot. Calculations based on Tauc equation reveal Eg(eV) for PPy/TiO2at 2.43and Ni/PPy/TiO2 at 2.12. The incorporation of Ni-NPs into the PPy/$TiO_2$ matrix successfully engineered a narrower optical band gap (2.12 eV vs. 2.43 eV). This reduction lowers the energy threshold for electron excitation, enhancing the material's responsiveness to visible light. Furthermore, the decreased band gap aligns with the measured enhancement in DC electrical conductivity a consequence of the formation of interconnected conductive networks by the dispersed Ni nanoparticles.

The X-ray Diffraction (XRD) spectra of PPy/TiO2-NCs, as shown in Fig. 1b, reveal characteristic diffraction peaks corresponding to 2θ (hkl) at 23.68° (101), 35.27° (004), 59.78° (200), 64.25° (204), 77.49° (220), and 87.44°, with respective d-spacings of 2.92 Å, 2.7 Å, 2.26 Å, 1.96 Å, 1.60 Å, and 1.39 Å. These peaks indicate the crystalline nature of the TiO2 within the composite. A broad diffraction peak at 20.32° corresponding to a d-spacing of 3.12 Å indicates the amorphous nature of the PPy component. The lattice parameters for the tetragonal structure were determined as a = 0.3784 nm and c/a = 2.5134 nm, with the unit cell volume (V) calculated to be 0.136 $nm^3$. The average crystallite size (D) was calculated 18.7 nm indicating the nanocrystalline nature of the PPy/TiO2composite. For S2the XRD spectra show characteristic diffraction peaks at 37.62° (004), 42.09° (111), 63.22° (200), and 76.14° (220), with respective d-spacings of 2.73 Å, 2.26 Å, 1.86 Å, and 1.39 Å. The unit cell volume (V) was calculated to be 0.133 $nm^3$.The average crystallite size (D) for the Ni-doped TiO2 nanoparticles was found to be 22.69 nm, indicating a slight increase in crystallite size due to nickel doping. Ni doping resulted in a measurable increase in crystallite size (from 18.7 nm to 22.69 nm), indicating modified $TiO_2$ crystal growth. Structural analysis confirmed both composites crystallize in a tetragonal phase, with Ni/PPy/$TiO_2$-NCs showing slight variations in lattice parameters while maintaining well-defined crystallinity.

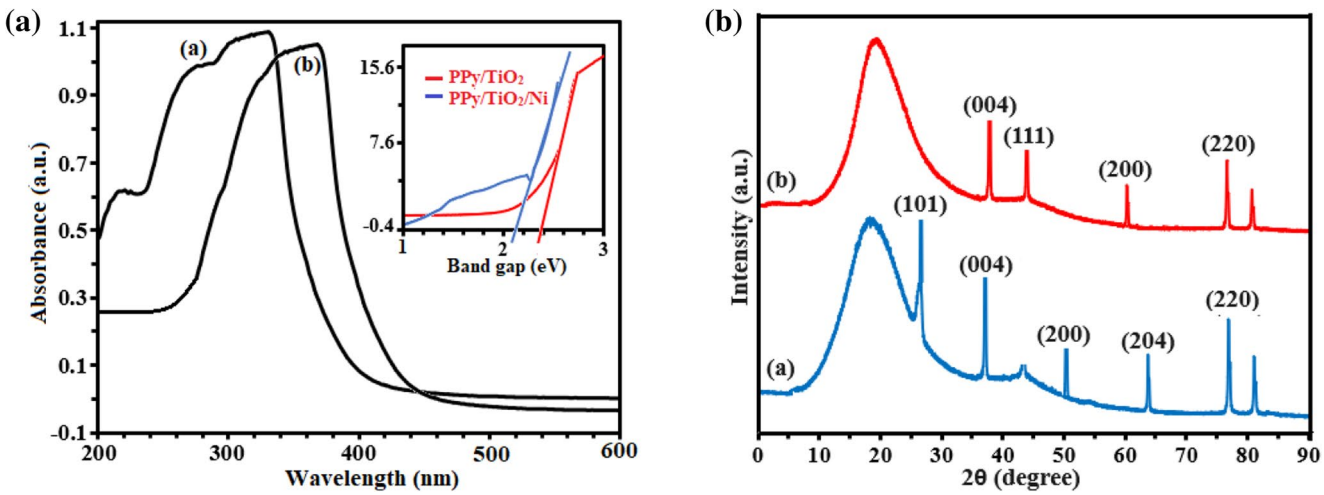


**Fig. 1** (**A**)UV absorbance and Tauc plot of (**a**) PPy/TiO2and (**b**) Ni/PPy/TiO2-NCs. (**B**) XRD spectra of (**a**) PPy/TiO2and (**b**) Ni/PPy/TiO2-NCs

### 4.2 Thermogravimetric Analysis

Thermal degradationof PPy/TiO2 has shown single step decomposition with TG onset at 244 °C leaving Wr 83.2% (Fig. 2). This was supported with a DTG signal at 219 °C with 27.0 µg/cel degradation rate. Prior to this temperature, PPy/TiO2 was decomposed leaving 98.3% Wr at 162 °C which is assigned to presence of 0.4% moisture content. Increase in temperature beyond 244 °C shows a rapid weight loss in PPy/TiO2 leaving Wr 74.2% at.

300 °C. The major decomposition of PPy/TiO2-NCs was observed in between 300–365°Chaving 88 µg/cel degradation rate at 350 °C. On further heating of PPy/TiO2 to 458 °C has contributed a marginal loss in weight leaving 18.6% Wr. The thermal degradation of Ni/PPy/TiO2-NCs shows one step decomposition with TGo at 301 °C leaving 91.1%Wr with.

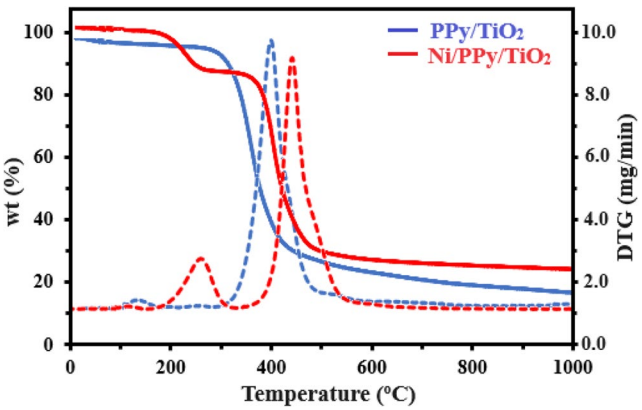


**Fig. 2** TG and DTG analysis of PPy/TiO2 and Ni/PPy/TiO2-NCs

54.0 µg/cel rate of decomposition at 370 °C. Prior to this temperature, Ni/PPy/TiO2-NCs was left Wr of 94.7% at 200 °C with 6.9 µg/cel rate of degradation at 183 °C. This may be assigned to the loss of moisture (1.8%) present in Ni/PPy/TiO2-NCs. Increase in temperature beyond 301 °C indicates a rapid weight loss in Ni/PPy/TiO2-NCs leaving 31.4% Wr at 400 °C. On increasing the temperature beyond 400 °C has shown a minor weight loss in Ni/PPy/TiO2- NCs leaving Wr 25.1% at 500 °C. No significant weight loss was observed beyond 600 °C. The distinct thermal behaviors originate from dual role of Ni: initially stabilizing the polymer matrix to delay decomposition, then catalyzing rapid PPy breakdown at elevated temperatures. Early mass loss in the Ni-doped sample is attributed to its higher moisture content. The stable residues after significant decomposition indicate that TiO2, possibly in conjunction with nickel, forms a thermally robust matrix that resist further degradation.

### 4.3 FT-IR Spectrum

In FT-IR spectra of PPy/TiO2-NCs, and Ni/PPy/TiO2-NCs several distinctive peaks can be observed (Fig. 3a). The peak at 3175 $cm^{-1}$ corresponds to the stretching vibration of O- H hydroxyl groups, indicating the presence of surface hydroxyls supported by existing literature. A bend vibration of coordinated H2O and Ti-OH is seen at 1575–1642 $cm^{-1}$, while the peak at 444 $cm^{-1}$ is attributed to the Ti-O bond vibration, characteristic of the TiO2 structure. Additionally, the O-O stretching mode for Ti-OOH on the surface appears at 676 $cm^{-1}$, confirming the presence of Ti-OOH groups. In the FT-IR spectra of both NCs, peaks at 3400 $cm^{-1}$ are

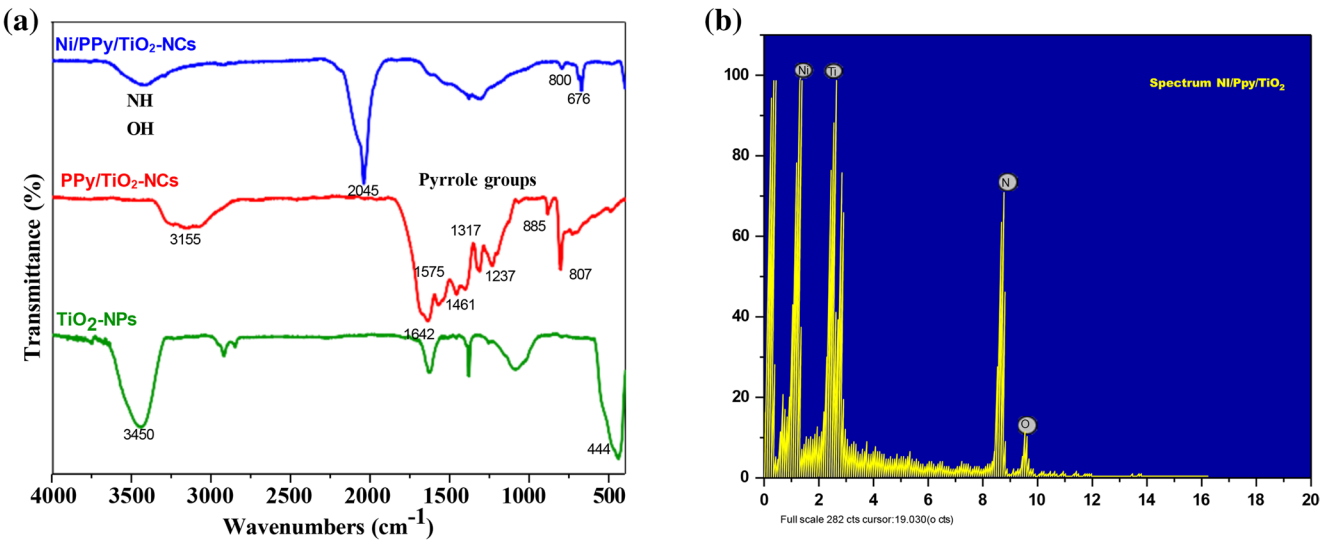


**Fig. 3** (**a**) FTIR spectra of NCs. (**b**) EDX of Ni/PPy/TiO2

attributed to the N-H bond stretching vibrations. These peaks indicate the presence of amino groups in the polymer structures consistent with reports on PPy-based composites. In the range of 1461 $cm^{-1}$, characteristic vibrations of the pyrrole rings are observed, which are fundamental to the PPy structure. Peaks at 1575 $cm^{-1}$, and 1642 $cm^{-1}$ correspond to the C-N bond stretching vibrations in PPy/TiO2-NCs and Ni/PPy/TiO2-NCs respectively. Moreover, specific peaks around 400 $cm^{-1}$ are related to the Ti-O bond vibrations in PPy/TiO2-NCs and Ni/PPy/TiO2-NCs. These FT-IR spectra provide valuable insights into the structural characteristics and compositions of the synthesized materials.

### 4.4 EDX

The EDX analysis results reveal the elemental composition of the synthesized materials in weight% (Fig. 3b). PPy is composed of 68.11% carbon and 31.89% nitrogen. In comparison, PPy/TiO2-NCs consist of 62.3% carbon, 15.08% nitrogen, 21.46% oxygen, and 1.17% titanium. Ni/PPy/TiO2-NCs show a composition of 54.11% carbon, 16.55% nitrogen, 25.97% oxygen, 3.26% titanium, and a minor 0.116% of nickel. These results illustrate the varied elemental compositions across the synthesized materials, reflecting the incorporation of titanium dioxide and nickel into the polymer matrix, which is essential for their functional properties in various applications.

| Weight% | C | *N* | O | Ti | Ni |
|---|---|---|---|---|---|
| **PPy** | 68.11 | 31.89 | - | - | - |
| **PPy/TiO2-NCs** | 62.3 | 15.08 | 21.46 | 1.17 | - |
| **Ni/PPy/TiO2-NCs** | 54.11 | 16.55 | 25.97 | 3.26 | 0.116 |

### 4.5 TEM

The transmission electron microscopy (TEM) studyreveals that PPy/TiO2–NCs exhibit a spherical morphology, displaying a nearly homogenous distribution of particles across the sample (Fig. 4a). However, some agglomeration of TiO2 particles on PPy conducting surface has shown due to cubic structure of TiO2.The average size of the synthesized PPy/TiO2-NCs ranges from 15 to 20 nm. Similarly, TEM analyses of Ni doped PPy/TiO2–NCs unveiled spherical shapes, consistent with those observed in PPy/TiO2–NCs **(**Fig. 4b**).** Average size of Ni/PPy/TiO2–NCs ranged from 16 to 24 nm, closely aligning with the dimensions of PPy/TiO2–NCs. Overall, both PPy/TiO2–NCs and Ni/PPy/TiO2–NCs demonstrated well-defined spherical morphologies with crystalline structures, as confirmed by XRD spectra. These finding highlights the successful synthesis and consistent structural characteristics of Ni/PPy/TiO2–NCs.

### 4.6 Electrical Conductivity

Electrical behaviour of PPy/TiO2–NCs was found in increasing order from1.12 to 2.32 mS/cm with increasing the voltage ranging from 1 to 100 V**(**Fig. 5**)**.To achieve the higher DC conductivity a critical amount of electrically conducting filler Ni is added into polymer matrix which builds a percolated conductive pathway throughout the composite material. The dispersion of Ni into PPy/TiO2 has been further substantiated by increase in their DC conductivity (mS/cm) irrespective to applied voltage ranging 1.0 to 100 V. The dispersion of Ni increases DC

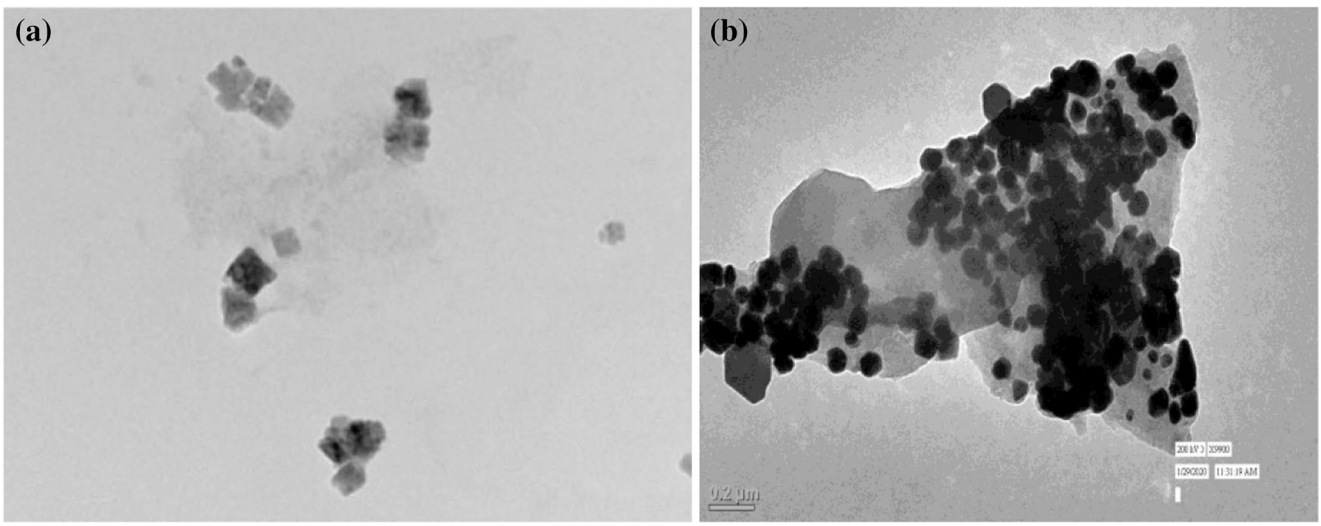


**Fig. 4** TEM study of (**a**) PPy/TiO2 and (**b**) Ni/PPy/TiO2–NCs

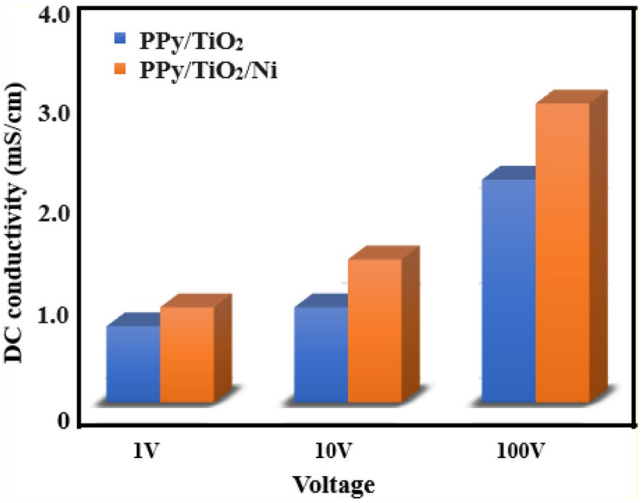


**Fig. 5** Effect of voltage on DC conductivity of PPy/TiO2 and Ni/PPy/TiO2

conductivity of PPy/TiO2 from 1.24 to 3.25 at 100 V. The enhanced electrical conductivity of Ni/PPy/TiO₂–NCs stems from the synergistic integration of its components. The homogeneous dispersion of conductive Ni-Npswithin the PPy matrix establishes efficient percolation pathways, directly contributing to the measured increase in DC conductivity. This improvement is electronically consistent with the reduced optical band gap (2.12 eV) determined from the Tauc plot, as a narrower band gap facilitates the thermal promotion and transfer of electrons from the valence to the conduction band. This dual evidence confirms that Ni incorporation effectively enhances the charge transport properties of the composite.

## 5 Photo Catalytical Dye Degradation Efficacy

The photocatalytic degradation of Rose Bengal (RB) dye was studied using TiO2, PPy/TiO2-NCs and Ni/PPy/TiO2 -NCs, as analysed by a UV-Visible spectrometer. The RB dye exhibits a maximum absorption wavelength (λ_max) at 543 nm. Initially, a high absorbance value was recorded, which gradually decreased upon exposure to sunlight, indicating dye degradation. Complete degradation of the dye was achieved when the absorbance value reached the baseline.The UV-Visible spectra showed that RB dye degraded by 79.57% in 4 min. The Ni/PPy/TiO2-NCs demonstrated superior performance, degrading 99% of the RB dye within the same timeframe. In comparison, the PPy/TiO2-NCs degraded 92.80% of RB dye in 4 min. These results indicate that Ni/PPy/TiO2-NCs possess enhanced photocatalytic properties compared to both PPy/TiO2-NCs and TiO2–NPs alone. The observed variations in photocatalytic efficiency can be attributed to differences in the band gap energies of the materials. TiO2 is a well-known photocatalyst with a band gap of approximately 3.2 eV, which allows it to absorb UV light but limits its efficiency under visible light. The incorporation of PPy, a conductive polymer reduces the band gap to 2.43 eV enhancing the absorption of visible light and improving the separation of photogenerated electron-hole pairs, thereby increasing photocatalytic activity. Further enhancement is observed with the incorporation of Ni into PPy/TiO2-NCs. Nickel doping introduces defect sites and additional energy levels within the band gap of TiO2 facilitating more efficient charge carrier separation and reducing recombination rates. This modification effectively narrows the band gap to 2.12 eV and extends the absorption range into the visible spectrum, thus significantly improving photocatalytic performance under sunlight. In conclusion, the superior photocatalytic degradation of RB dye by PPy/TiO2-NCs and Ni/PPy/TiO2- NCs and TiO2-NPs can be scientifically explained by the band gap modifications and improved charge carrier dynamics introduced by the PPy and Ni dopants. This enhanced photocatalytic activity highlights the potential for efficient environmental remediation applications.

In Fig. 6a-f, the degradation curves of RB dye as a function of irradiation time for PPy/TiO2 and Ni-doped PPy/TiO2-NCs at pHs of 5, 10, and 13, along with the related rate constants, are shown. By varying the pH of the solution, the charge on the catalyst surface is altered. The pH-dependence of photocatalytic degradation is governed by electrostatic interactions between the catalyst surface and dye molecules, mediated by the point of zero charge (PZC) of the semiconductor. For TiO2, the PZC is around 6–7. RB dye is cationic, and its degradation rate increases with increasing pH due to the enhanced interaction with the negatively charged catalyst surface. In an acidic solution (pH < PZC), the TiO2 photocatalyst surface develops a positive charge, which inhibits RB dye adsorption due to electrostatic repulsion. The maximum degradation occurs under visible light irradiation for PPy/TiO2 and Ni-doped PPy/TiO2 at pH 10, achieving optimal degradation within 180 min of irradiation. The addition of TiO2 catalyst enhances the degradation rate of RB dye, primarily due to increased adsorption of dye molecules on the catalyst surface. The higher photocatalytic activity is attributed to the electrostatic attraction between the positively charged dye molecules and the negatively charged TiO2 surface. Conversely, as pH increases from 10 to 13, the degradation percentage decreases, with colour removal decreasing from 99% to 87%. In an alkaline environment (pH > PZC), the TiO2 surface becomes negatively charged, and RB dye typically exists in its un-ionized neutral form.

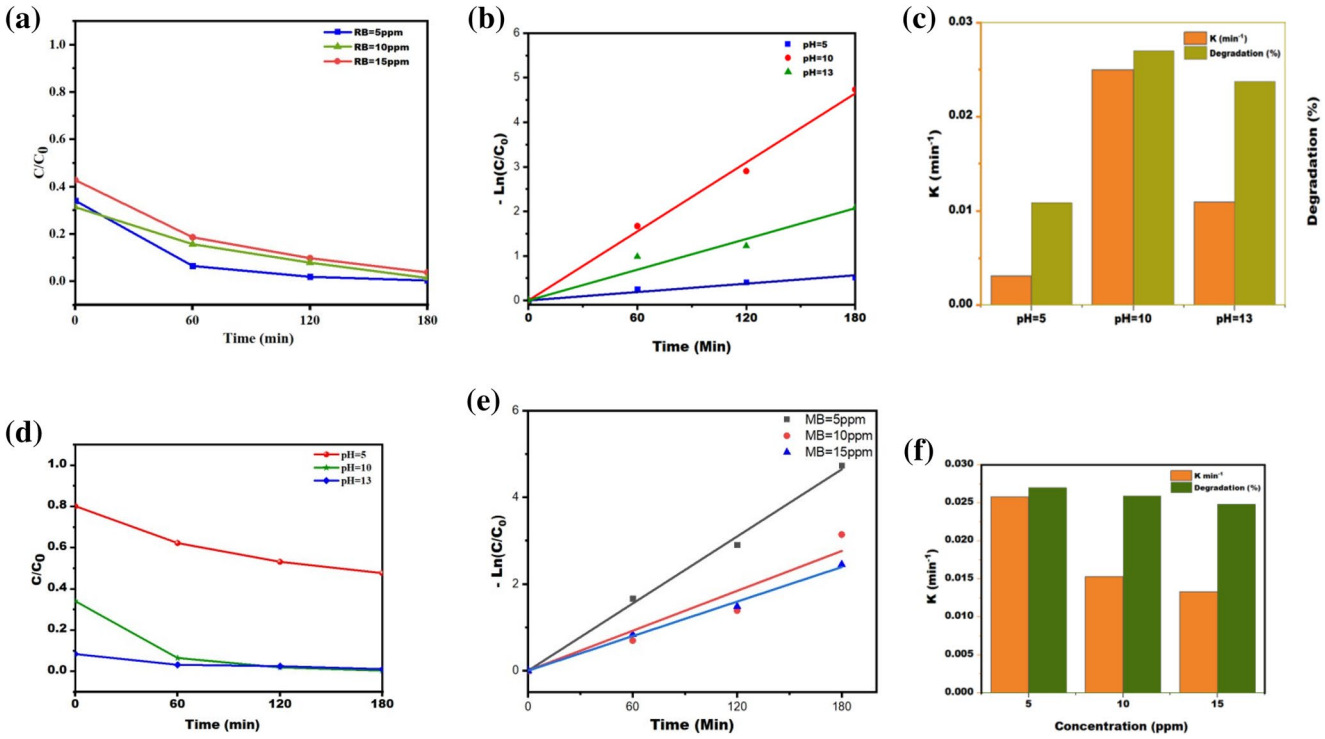


**Fig. 6** Degradation of RB dye over time under UV irradiation for (**a**–**c**) PPy/$TiO_2$ and (**d**–**f**) Ni-doped PPy/$TiO_2$ nanocomposites at pH values of 5, 10, and 13. The corresponding degradation rate constants for each system are also presented

The photocatalytic efficiency is controlled by electrostatic attraction between the cationic RB dye and the catalyst surface. At pH 10 (>$TiO_2$'s PZC), the negatively charged surface maximizes dye adsorption. At pH 5, a positive surface repels the dye. At pH 13, RB becomes neutral and $Na^+$ ions compete for sites, reducing adsorption. Ni-doping enhances performance at all pH by improving charge separation and light absorption. Figure 6c and f displays the reaction rate constants and dye degradation percentages at different pH values for PPy/TiO2 and Ni-doped PPy/TiO2 nanocomposites. The variations in degradation rates and percentages with pH are explained by the changes in surface charge of the TiO2 catalyst, affecting dye adsorption and the availability of active sites for photocatalytic degradation.

## 6 Electrochemical Degradation of RB Dye

The redox behaviour of RB dye was investigated using cyclic voltammetry (CV) on glassy carbon electrode (GCE) in a 0.1 M KOH solution at pH 8.0, with a potential range of −1.6 V to.

0.15 V and scan rates from 5-15mV/s. CV analysis(Fig. 7a) assessed the anodic (Epa) and cathodic (Epc) peak potentials and their corresponding peak currents (Ipa and Ipc). Results indicated that increasing the scan rate led to a rise in Ipa from 0.5 to 1.5 mA and a shift in Epa from −0.93 to −0.72 V, while Ipc and Epc decreased from −1.0 to −1.63 mA and −1.2 to −1.3 V, respectively. Further, RB dye degradation was quantified using PPy/TiO2 and Ni/PPy/TiO2 photocatalytic plate (PCPs) under UV irradiation in 30 mL of 100 ppm RB solution. The RB solution was exposed to UV irradiation with controlled energy at $65.80 \times 10^{-17}$Ws, over incubation periods from 10 to 30 min. Post-irradiation, the residual RB concentration was measured through CV analysis. Figure 7b and c show a progressive decline in peak currents with increased irradiation time for both PCPs, achieving complete degradation of the 100 ppm RB solution. Notably, Ni/PPy/TiO2 PCPs demonstrated superior degradation efficiency99.5%, completely eliminating the RB redox peak under similar conditions. The enhanced photocatalytic performance is attributed to the synergistic effects of Ni incorporation. The homogeneous dispersion of Ni-NPs within the PPy/$TiO_2$ matrix improves charge transfer and separation, while the reduced optical band gap (2.12 eV) significantly enhances visible light absorption. Together, these factors minimize electron-hole recombination and generate more reactive species, highlighting the superior potential of Ni/PPy/$TiO_2$ nanocomposites for efficient photodegradation.

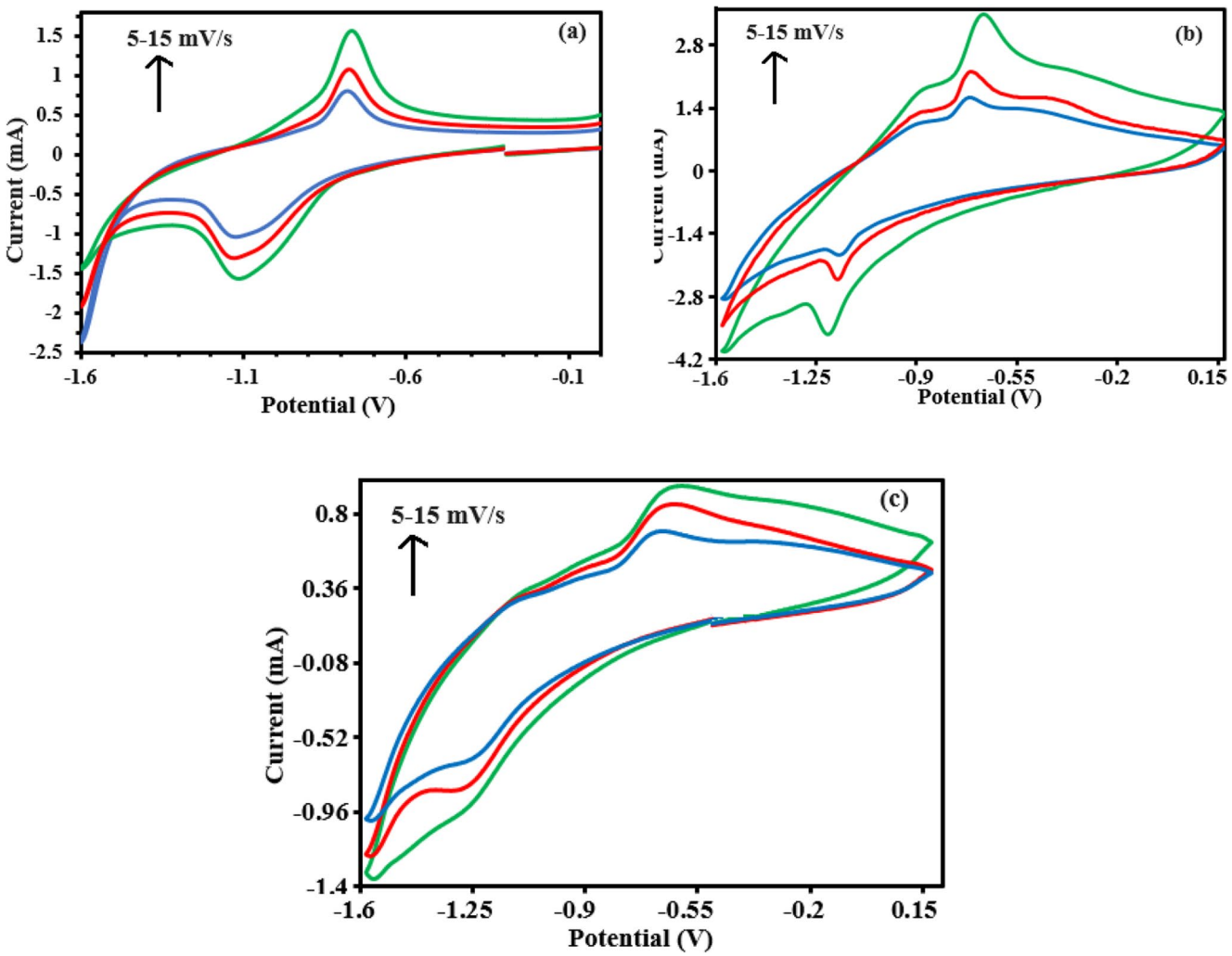


**Fig. 7** V of RB (**a**), and CV of degradation of RB through (**b**) PPy/TiO2, (**c**) Ni/PPy/TiO2

## 7 Conclusion

This study successfully synthesized Ni/PPy/TiO2–NCs using sustainable methods, addressing global challenges related to e-waste management and wastewater treatment. Nickel nanoparticles were derived from discarded batteries, while TiO2 nanoparticles were synthesized from sugarcane husk, ensuring an environmentally friendly approach. The Ni/PPy/TiO2–NCs exhibited a significantly reduced optical band gap of 2.12 eV, high thermal stability with decomposition temperatures exceeding 450 °C, and enhanced DC conductivity. In photocatalytic degradation tests, Ni/PPy/TiO2–NCs achieved 99.5% degradation of Rose Bengal dye under sunlight within 4 min, compared to 92% by PPy/TiO2-NCs and 79.57% by TiO2 alone. Electrochemical degradation experiments demonstrated complete degradation within 30 min, outperforming the 92% and 79.57% degradation rates of PPy/TiO2-NCs and TiO2, respectively. The enhanced performance is attributed to the synergistic effects of Ni and PPy incorporation, which optimize charge carrier dynamics and reduce recombination rates. These modifications significantly improve the photocatalytic and electrochemical degradation efficiencies of the nanocomposites. In conclusion, the synthesized Ni/PPy/TiO2– NCsoffer a promising, multifunctional solution for environmental remediation, addressing e- waste and wastewater challenges. Their superior degradation capabilities, combined with sustainable synthesis methods, underscore their potential in advancing green nanotechnology and promoting environmental sustainability.

**Funding** No funding was received for this work.

## Declarations

**Ethical Approval** Not applicable.

**Consent for Publication** Not applicable.

**Conflict of interest** The authors declare no conflict of interest.

## References


1. Ghulam ST, Abushammala H (2023) Challenges and opportunities in the management of electronic waste and its impact on human health and environment. Sustainability 15(3):1837
2. Shittu OS, Williams ID, Shaw PJ (2021) Global e-waste management: can WEEE make a difference? A review of e-waste trends, legislation, contemporary issues and future challenges. Waste Manag 120:549–563
3. Vaish B (2020) E-waste and their implications on the environment and human health. E- waste Recycling and Management: Present Scenarios and Environmental Issues. pp 219–232
4. Saha L et al (2021) Electronic waste and their leachates impact on human health and environment: global ecological threat and management, vol 24. Environmental Technology & Innovation, p 102049
5. Islam A et al (2020) Advances in sustainable approaches to recover metals from e-waste-a review. J Clean Prod 244:118815
6. Islam A et al (2021) Advances in physiochemical and biotechnological approaches for sustainable metal recovery from e-waste: a critical review. J Clean Prod 323:129015
7. Nahiun KM et al (2021) A review on the methods of industrial waste water treatment. Sci Rev 7(3):20–31
8. Mamidi N et al (2024) Multifaceted hydrogel scaffolds: bridging the gap between biomedical needs and environmental sustainability. Adv Healthc Mater. https://doi.org/10.1002/adhm.202401195
9. Kumar A et al (2024) Revolutionizing the biomedical and environmental clean-up through polymeric nano-sponges: a review. Nano-Struct Nano-Objects 39:101193
10. Aazza M, Ahlafi H (2024) Investigation of m-NP and p-NP adsorption from single and binary aqueous solutions onto Al2O3 and HDTMA+/Al2O3 composite using first derivative UV/Visible spectrophotometry. J Mol Liq. https://doi.org/10.1016/j.molliq.2024.124220
11. Khokhar S, Anand H, Chand P (2022) Current advances of nickel based metal organic framework and their nanocomposites for high performance supercapacitor applications: a critical review. J Energy Storage 56:105897
12. Dravid SV et al (2020) Nickel nanoparticle-filled high-performance polymeric nanocomposites for EMI shielding applications. J Electron Mater 49:1630–1637
13. Hao L, Yu D (2022) Progress of conductive polypyrrole nanocomposites. Synth Met 290:117138
14. Golkhatmi SZ et al (2021) Structural properties and supercapacitive performance evaluation of the nickel oxide/graphene/polypyrrole hybrid ternary nanocomposite in aqueous and organic electrolytes. Energy 214:118950
15. Ainali NM et al (2021) Insights into biodegradable polymer-supported titanium dioxide photocatalysts for environmental remediation. Macromol 1(3):201–233
16. Chen Y et al (2024) Directional regulation of reactive oxygen species in titanium dioxide boosting the photocatalytic degradation performance of azo dyes. J Colloid Interface Sci. https://doi.org/10.1016/j.jcis.2024.06.081
17. Monteagudo J et al (2020) Effect of reduced graphene oxide load into TiO2 P25 on the generation of reactive oxygen species in a solar photocatalytic reactor. Application to antipyrine degradation. Chem Eng J 380:122410
18. Khan ZUH et al (2023) Removal of organic pollutants through hydroxyl radical-based advanced oxidation processes. Ecotoxicol Environ Saf 267:115564
19. Chan KH et al (2021) Closed-loop recycling of lithium, cobalt, nickel, and manganese from waste lithium-ion batteries of electric vehicles. ACS Sustain Chem Eng 9(12):4398–4410
20. Blumbergs E et al (2021) Cadmium recovery from spent Ni-Cd batteries: a brief review. Metals 11(11):1714
21. Perera MC, Rienzie R, Adassooriya NM (2022) Sustainable Production of Nanomaterials from Agricultural Wastes. Agricultural and Kitchen Waste. CRC Press, pp 83–104
22. Jain P et al (2023) Functionalization of sugarcane bagasse–based paper with amla pomace/titanium dioxide nanoparticles providing antimicrobial protection for food safety. Biomass Convers Biorefin 14:1
23. Pang Y et al (2021) *Photocatalytic degradation of malachite green using titanium dioxide immobilised on oil palm empty fruit bunch derived cellulose.* Materials Today: Proceedings, 46: pp. 2017–2023
24. Lin TH et al (2023) Synthesis of TiO2-doped carbon aerogel from sugarcane bagasse for high efficiency of photodegradation of methylene blue in the water. Vietnam J Chem 61(2):227–237
25. Ghazzy A, Naik R, Shakya A (2023) *Metal–Polymer Nanocomposites: A Promising Approach to Antibacterial Materials. Polymers* 15, 2167. 2023


**Publisher's Note** Springer Nature remains neutral with regard to jurisdictional claims in published maps and institutional affiliations.

Springer Nature or its licensor (e.g. a society or other partner) holds exclusive rights to this article under a publishing agreement with the author(s) or other rightsholder(s); author self-archiving of the accepted manuscript version of this article is solely governed by the terms of such publishing agreement and applicable law.